

Understanding $B^0 \rightarrow D^+ NN$ and Its Implications

Chun-Khiang Chua, Wei-Shu Hou and Shang-Yuu Tsai

Department of Physics, National Taiwan University, Taipei, Taiwan 10764, R.O.C.
(December 25, 2018)

The CLEO Collaboration recently reported the observation of the $B^0 \rightarrow D^+ pn$ mode at a rate only a factor of 4.5 lower than $B^0 \rightarrow D^+ \pi^+$ and $D^+ \pi^+$. We try to understand this with a factorization approach by assuming color transparency for nucleon pairs. The baryon weak vector current form factors are related by isospin rotation to nucleon electromagnetic form factors. By using $G_M^{p,n}$ measured from $e^+e^- \rightarrow NN$ and $pp \rightarrow e^+e^-$ processes, we are able to account for up to 60% of the observed rate. A vector meson dominance picture may serve as a link to the $B^0 \rightarrow D^+ \pi^+$ process, where the proximity of rates and the validity of color transparency can be interpreted. The model is then applied to B decays to other mesons plus pn modes and D^+ plus strange baryon pairs.

PACS numbers: 13.25.Hw, 13.40.Gp, 14.20.Dh

I. INTRODUCTION

Following a suggestion by Dunietz [1] that $B^0 \rightarrow D^+ NN$ decays are likely sizable, the CLEO Collaboration has recently reported the first observation of such modes [2]:

$$\text{Br}(B^0 \rightarrow D^+ pn) = (14.5^{+3.4}_{-3.0} \text{--} 2.7) \times 10^{-4}; \quad (1)$$

$$\text{Br}(B^0 \rightarrow D^+ pp^+) = (6.5^{+1.3}_{-1.2} \text{--} 1.0) \times 10^{-4}; \quad (2)$$

Although the decay final states are three or four-body, they are only a few times below typical two-body mesonic modes [3], e.g.

$$\text{Br}(B^0 \rightarrow D^+ \pi^+) = (6.8 \text{--} 3.4) \times 10^{-3}; \quad (3)$$

$$\text{Br}(B^0 \rightarrow D^+ \pi^0) = (2.76 \text{--} 0.21) \times 10^{-3}; \quad (4)$$

Since D^+ creation carries away much energy, the observed large rate of $B^0 \rightarrow D^+ pn$ supports the suggestion that enhanced baryon production is favored by reduced energy release on the baryon side [4]. Thus, given the large rate of $B^0 \rightarrow X_s$ decay where $p_0 > 2 \text{ GeV}$ [5], the $B^0 \rightarrow p$ decay may be sizable [4] compared to charmless two-body baryonic modes. Similar argument holds for $B^0 \rightarrow p$ as implied by $B^0 \rightarrow X_s$. With the help of spin information from $\pi^0 p$ decay, the observation of such charmless three (or more) body baryonic modes involving baryons allows for a search program for triple-product type of CP and T violating effects. Thus, a better understanding of the $B^0 \rightarrow D^+ pn$ decay is not only worthwhile in its own right, it can also serve as an important first step towards a more ambitious project on charmless baryonic modes.

In order to account for the proximity of rates shown in Eqs. (1) and (3), $B^0 \rightarrow D^+ pn$ was seen through a simple pole model [4] as occurring in two steps: $B^0 \rightarrow D^+ h$ followed by $h \rightarrow NN$, where h stands for the ρ -shell $^+$ and 0 mesons. The strong interaction hNN vertex allowed for qualitatively understanding that a three-body decay such as $B^0 \rightarrow D^+ pn$ could have rate comparable to the two-body $B^0 \rightarrow D^+ \pi^+$ decay. Because of

the strong dependence on the meson-nucleon form factors (where we lack good understanding of momentum scales involved), however, the pole model can be quite arbitrary. We therefore turn to a different approach by proposing a factorization scheme based on the color transparency of the produced nucleon pair pn . The three-body decay is seen as generated by two factorized weak currents (linked by a W^- boson), where one current converts B^0 into D^+ and the other creates the nucleon pair.

It is well known that the vector portion of the weak current and the isovector component of the electromagnetic (em) current form an isotriplet. Thus, information on the nucleon em form factors, for which much data exist in both the space-like region [6] (e.g. $ep \rightarrow ep$), and, of particular interest to us, the time-like region [9,8,7,10] (e.g. $e^+e^- \rightarrow NN$ and $pp \rightarrow e^+e^-$), can be transferred to the nucleon weak form factors by a simple isospin rotation. The total decay amplitude that comes from the vector portion of the weak current can be written down unambiguously and the portion of the branching fraction that comes solely from the weak vector current can be readily obtained once the form factors are given. We find that the vector current can account for 50% (60% of the observed rate of Eq. (1)). Since this analysis involves just the factorization hypothesis but is otherwise based on data, it is rather robust.

Although the axial vector and vector current contributions interfere in the decay amplitude, the interference vanishes when one sums over spin and integrates over phase space. The total rate is therefore a simple sum of the contributions from the vector and axial vector portions of the weak nucleon form factor. Like the vector case, we could in principle obtain the axial vector contribution if the nucleon form factors of the axial current were known. Unfortunately, the time-like data is still lacking, hence the contribution from this part remains undetermined. In spite of this, a rough estimate can still be given, which seems to be the right amount. We point out, however, that information on the time-like nucleon axial form factor could in fact be obtained in the future via the $B^0 \rightarrow D^+ pn$ decay data. One just has to sepa-

rate the axial vector contribution from the vector part.

To gain further insight, in part with an eye towards future studies of charmless baryonic modes, we extend the pole model approach to include higher resonances by invoking Vector-Meson-Dominance (VMD), which states that a photon couples to hadrons only via intermediate vector mesons. Only the isovector ones are relevant to us. The electromagnetic weak vector form factors are specified via a dispersion relation by constructing the proper spectral functions, which are then truncated to a few vector meson poles. This enables us to picture the three-body process as an improved pole model, where a B^0 first becomes a D and an on-shell vector meson, and the latter then generates the pn nucleon pair in the final state. In order to reproduce the asymptotic form of the electromagnetic form factors predicted by perturbative QCD and to agree better with data, a fictitious pole is introduced to mimic the influence of higher resonances and continuum. It should be stressed that the improved VMD pole model differs from a simple pole model not only by the number of poles, but by enforcing the correct asymptotic behavior predicted by perturbative QCD.

Our starting assumption of color transparency of the nucleon pair in the factorization approach can be interpreted, hence partially justified, from the VMD pole model perspective.

This paper is organized as follows: in the next section we describe the simple pole model approach and discuss the possible difficulties inherent in this model. In Sec. III, we take a more general point of view by making a factorization assumption, which allows us to relate the vector current contribution to the nucleon electromagnetic form factors that enjoy abundance of experimental data. The axial vector contribution is also estimated. We then introduce the VMD approach in Sec. IV as an improved pole model. Finally, we apply our analysis to $B^+ \rightarrow D^{(*)}pn$ and $B^0 \rightarrow D^{(*)}pn$ as well as other baryonic modes containing strangeness. We conclude in the last section.

II. NAIVE POLE MODEL

The three-body decay $B^0 \rightarrow D^{(*)}pn$ occurs in two steps in the pole model, which we depict in Fig. 1: the B meson first decays into D plus $^+$ or $^+$, which then transforms into the nucleon pair. That is, there are two vertices in the pole model, one for the two-body B decay and the other for the meson-nucleon interaction.

For the first vertex, the appropriate theoretical framework is an effective theory involving the Wilson operator product expansion obtained by integrating out the heavy degrees of freedom. The approach which has often been employed in nonleptonic heavy hadron decays is based on factorization, which holds in the limit that one can ignore soft non-perturbative effects. The rationale lies in the so-called color transparency [1], in which one expects intuitively that a pair of fast moving (energetic)

quarks in a color-singlet state effectively decouples from long-wavelength gluons. For $B \rightarrow h_1 h_2$ decays where typically $E_{h_{1,2}} \sim O(m_B/2)$, the energy of the quarks leaving the interaction is large hence soft final state interactions should be small, and factorization should be a good approximation.

With the factorization ansatz, the matrix element of B^0 decaying into D plus say, $^+$, can be expressed as a product of two factors, $\langle D | j_V | B^0 \rangle \langle ^+ | j_A | 0 \rangle$, where $V = A$ is the weak current. With the $^+$ meson subsequently producing the nucleons via strong interactions, the decay amplitude of $B^0 \rightarrow D^{(*)}pn$ can be readily written down

$$iM = i \frac{G_F}{2} V_{ud} V_{cb} a_1 \langle D | j_V | B^0 \rangle \langle ^+ | j_A | 0 \rangle$$

$$= i \frac{g + \frac{q \cdot q}{m^2}}{q^2 - m^2} \langle D | j_V | B^0 \rangle \langle ^+ | j_A | 0 \rangle$$

$$= i \frac{2u p_p \cdot q_1^{NN} + \frac{i g_2^{NN}}{2m_N} q \cdot v_{pn}}{q^2 - m^2} \langle D | j_V | B^0 \rangle \langle ^+ | j_A | 0 \rangle; \quad (5)$$

where the transition matrix element is

$$\langle D | j_V | B^0 \rangle = \frac{2V(q^2)}{m_B + m_D} \langle D | j_V | B^0 \rangle$$

$$= i g \frac{q \cdot q}{q^2} (m_B + m_D) A_1(q^2)$$

$$+ i (p_B + p_D) \cdot \frac{m_B^2 - m_D^2}{q^2} q \frac{A_2(q^2)}{m_B + m_D} q$$

$$+ i 2m_D \frac{q \cdot q}{q^2} A_0(q^2); \quad (6)$$

$q = p_B - p_D = p_p + p_n$ is the momentum transfer (so $t = q^2$ is nothing but the pn pair mass), D is the polarization of the D meson, and g_1^{NN} and g_2^{NN} are respectively the vector (Dirac) and tensor (Pauli) coupling constants of the meson to the nucleons.

The probability amplitude in Eq. (5) consists of two major parts which correspond to the two vertices analyzed by the pole model. The first factor $\langle D | j_V | B^0 \rangle$

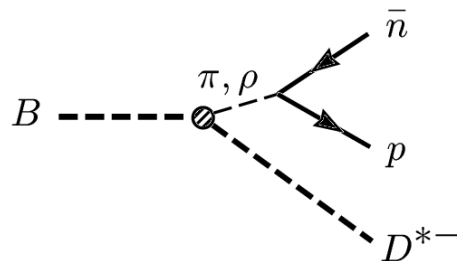


FIG. 1. The pole model for $B^0 \rightarrow D^{(*)}pn$:

A β^0 if m describes the $b \rightarrow c$ transition vertex where form comes from the creation of the meson. The ω shell π^+ then propagates to couple to the nucleon pair via the strong interaction, which is described by the vector and tensor couplings in the last factor of Eq. (5). For decays via other mesons, one can get the corresponding decay amplitude by simple substitutions.

The matrix element $\langle \psi | A \beta^0 | i \rangle$ involves the $B \rightarrow$ vector meson form factors [12] $V(q^2)$, $A_0(q^2)$, $A_1(q^2)$ and $A_2(q^2)$. We shall use the BSW [13,14] and the light-front (LF) [15] form factor models in our calculation. As we shall see, because of the relatively large mass of the $b\bar{c}$ bound state in $b \rightarrow c$ transition as compared to the momentum transfer, the results do not depend strongly on the form factor model. The CKM matrix elements V_{ud} and V_{cb} are taken to be 0.9757, 0.039 respectively, and the decay constant $f = 216 \text{ MeV}$. The factorization scheme depends on a further quantity $a_1 = c_1 + c_2/N_c$, with N_c the number of quark colors in "naive factorization" and $c_{1,2}$ are Wilson coefficients. The effective coefficient a_1 can be extracted from experiment. We follow Ref. [16,18] to get the value of a_1 from fitting the corresponding 2-body decays. We find $a_1^{BSW} = 0.87$ and $a_1^{LF} = 0.75$, respectively, for the BSW and the LF form factor models. These numbers are consistent with $a_1^{BSW} = 0.86 \pm 0.21$ and $a_1^{LF} = 0.74 \pm 0.18 \pm 0.06$ given in Ref. [18], but smaller than $a_1 = 1.03$ from naive factorization, implying nonfactorizable effects could be at (20–30)% level.

The last factor of Eq. (5) describes the π^+ -nucleon interaction in terms of strong nucleon form factors. In order to demonstrate the strong model dependence, let us consider, for example, the following two ad hoc substitutions:

Type I:

$$g_1^{NN} \rightarrow g_1^{NN}(q^2) = g_1^{NN} \frac{2 - m^2}{2 + q^2}; \quad (7)$$

$$g_2^{NN} \rightarrow g_2^{NN}(q^2) = 6.1 g_1^{NN}(q^2); \quad (8)$$

where Λ is the cutoff parameter, and, in contrast

Type II:

$$g_1^{NN} \rightarrow g_1^{NN}(q^2) = g_1^{NN} \frac{2 + m^2}{2 + q^2}; \quad (9)$$

$$g_2^{NN} \rightarrow g_2^{NN}(q^2) = 6.1 g_1^{NN}(q^2); \quad (10)$$

The parameters g_1^{NN} and Λ are from Table B.1 of Ref. [19], initially for purpose of space-like form factors. The branching fraction results Br for these coupling constants are listed in Table I.

We see from Table I that all numbers exceed the experimental value in Eq. (1). The "\|" in the table corresponds to an artificial blow-up in rate, which results from the integration of momentum transfer over the cutoff energy $Q^2 = 2.2 \text{ GeV}^2$. Furthermore, from the above

TABLE I. Branching fraction of $B^0 \rightarrow D^+ \pi^-$ via $\pi^+ \rightarrow \pi^0 \pi^+$ pn with BSW hadronic form factors.

g_1^{NN}	(GeV)	Br (Type I)	Br (Type II)		
			$n=0$	$n=1$	$n=2$
3.72	1.3	0.034	0.621	0.044	0.004
3.36	1.4	0.051	0.508	0.043	0.004
2.97	2.2		0.395	0.083	0.019

Table we find that for the Type II form factors, although the results do not vary too much for each given power n , they do sensitively depend on the power of the form factors for each given set of g_1^{NN} and Λ . We note also that Br obtained by using the monopole ($n=1$) Type II form factors are compatible with those obtained from the Type I form factors.

The pole model provides at best only a qualitative understanding of the large rate of the three-body mode in terms of the strong dynamics involved in the NN system. But the quantitative results based on this model is highly unreliable, largely because of our ignorance of time-like meson-nucleon couplings. Since the form factors, the coupling g_1^{NN} and the cutoff Λ^2 are extracted from low Q^2 ($Q^2 < q^2$) space-like processes, they cannot be expected to give reliable quantitative results for time-like processes at higher energies.

For decay through the exchange of π^+ -meson, since the amplitude does not interfere with that of the meson after summing over the nucleon spins, one can calculate it separately. According to the argument given in Ref. [20], we have $g^{NN} = g^{NN} \Lambda^2 = 13$, where g^{NN} is the value of the pion-nucleon space-like form factor at $q^2 = 0$, and g^{NN} is the time-like form factor evaluated at the NN -threshold. A simple calculation using constant $g^{NN} = g^{NN} \Lambda^2 = 13 = 1.1$ with $g^{NN} = 14.4$ taken from Table B.1 of Ref. [19], gives branching fractions for both the light-front and BSW models at the 10^{-5} level, which are 2 orders of magnitude smaller than the experimental value in Eq. (1). This can be viewed as an upper bound for us to safely ignore the π^+ contribution.

We remark that $Br(B^0 \rightarrow D^+ \pi^-) = (1.30 \pm 0.27)\%$ is about twice the strength of $Br(B^0 \rightarrow D^+ \pi^-)$. Its contribution to $Br(B^0 \rightarrow D^+ \pi^-)$ cannot be easily evaluated in this pole model approach, because of lack of information on the related strong couplings.

III. FACTORIZATION APPROACH AND NUCLEON FORM FACTOR DATA

Let us extend factorization to the three-body decay by assuming color transparency of the $\pi^0 \pi^+$ pair

$$\langle D^+ \pi^0 | j_{eff} \beta^0 | i \rangle = \frac{G_F}{\sqrt{2}} V_{ud} V_{cb} a_1 \langle D^+ | j | A \beta^0 | i \rangle$$

$$i u(p_p) \gamma^\mu v(p_n) = u(p_p) \left[\frac{h}{2m_N} \gamma^\mu + (\not{p}_n - \not{p}_p) \gamma^\mu \right] v(p_n); \quad (22)$$

The terms proportional to q in Eq. (6) vanish in the limit of equal proton and neutron mass. For completeness, the amplitude for nucleons generated by the axial vector current is given by

$$i M_A = \frac{G_F}{\sqrt{2}} V_{ud} V_{cb} a_1 h_D \not{J} \not{A} \not{B}^0 i \\ u(p_p) \gamma_A(t) \not{5} + \frac{h_A(t)}{2m_N} q \not{5} v(p_n); \quad (23)$$

where $h_D \not{J} \not{A} \not{B}^0 i$ is given in Eq. (6).

The two amplitudes M_A and M_V interfere, since

$$2 \text{Re}(M_A M_V) = 32 G_F^2 \not{J}_{ud} \not{J}_{cb} a_1^2 \\ \int d^3 p_B \int d^3 p_D \int d^3 p \int d^3 p' \gamma_A(t) V(t) A_1(t) G_M^p(t) G_M^n(t) \quad (24)$$

is in general non-vanishing. The summation is performed with respect to the spins of the nucleons and the polarizations of D^0 . The three-body phase space is described by the two independent variables $m_{pn}^2 = (p_p + p_n)^2$ and $m_{Dn}^2 = (p_D + p_n)^2$. The interference term is antisymmetric with respect to exchange of p_p and p_n . For given t , as we integrate over the kinematically allowed m_{Dn}^2 , each value of $2 \text{Re}(M_A M_V)$ from a given pair of p_p, p_n would be cancelled by those from the exchanged pair. The interference term thus contributes nothing to the total three body decay rate, and the final result is a simple sum of the contribution from M_V and M_A separately.

It is interesting to note that, although the effect of $2 \text{Re}(M_A M_V)$ does not show up in the decay rate, we can nevertheless construct an asymmetry ratio measurable based on the antisymmetric nature of this quantity, to extract the time-like information of $g_A(t)$ from $B^0 \rightarrow D^0 p n$ data. The information of $V(t), A_1(t)$ and $G_M^p(t)$ in Eq. (24) can be found by other means, and the overall factors a_1 and $\not{J}_{ud} \not{J}_{cb}$ would cancel in the asymmetry ratio.

B. Form Factor Data and Perturbative QCD

Much data has been accumulated for the nucleon electromagnetic form factors, which turns the vector portion of the decay amplitude $i M_V$ expressed in Eq. (21) into something that we can handle. The branching fraction contributed from the vector current can be readily obtained once the nucleon electromagnetic form factors are given, thanks to the isospin relation of weak vector and electromagnetic currents. We note further that care has to be taken to make sure that

the form factors satisfy the constraint from perturbative QCD (PQCD).

The so-called quark counting rules [21] give the leading power in the large- q^2 fall-off of the form factor $F_1(t)$ by counting the number of gluon exchanges which are necessary to distribute the large photon momentum to all constituents. Since helicity- \perp leads to an extra $1=t$ factor in $F_2(t)$, one finds, in the limit $q^2 \rightarrow \infty$

$$F_i(t) \sim (q^2)^{-(i+1)} \ln \frac{q^2}{Q_0^2}; \quad i = 2 + \frac{4}{3}; \\ i = 1; 2 \quad (25)$$

where α_s is the α_s function of QCD to one loop and Q_0 is a QCD scale parameter $\approx 0.3 \text{ GeV}$. We note that α_s depends weakly on the number of flavors; for three flavors $\alpha_s = 2.148$.

The asymptotic form given in Eq. (25) has been confirmed by many experimental measurements of the nucleon $G_M = F_1 + F_2$ over a wide range of momentum transfers in the space-like region. The asymptotic behavior for G_M^p also seems to hold in the time-like region, as reported by the Fermilab E760 experiment [7] for $8.9 \text{ GeV}^2 < t < 13 \text{ GeV}^2$. A another Fermilab experiment, E835 [9], has recently reported G_M^p form factor transfer up to 14.4 GeV^2 . It also provides support for the asymptotic form of G_M^p and gives an empirical fit [9]:

$$G_M^p(t) \sim \frac{C}{t^2 \ln \frac{t}{Q_0^2}}; \quad (26)$$

which agrees well with the asymptotic form in Eq. (25).

By exploiting the relation in Eq. (17), the combination $2(F_1^V + F_2^V)$ in Eq. (21) can be replaced by $G_M^p - G_M^n$ which is composed of measurable quantities. Similar replacement can also be made for F_2^V , which is a combination of $G_M^p - G_E^p$ and $G_M^n - G_E^n$. Most time-like data for the magnetic form factors, however, are extracted by assuming either $F_E^j = F_M^j$ or $F_E^j = 0$ in the region of momentum transfer explored. Since $G_M - G_E = (1 - t/4m_N^2) F_2$ clearly vanishes at threshold, the absence of clear deviation from this assumption in extracting data implies the contribution of F_2 is negligible even for t far beyond the threshold, which is consistent with the prediction from QCD. In fact, by assuming $F_E^j = F_M^j$ in extracting G_M from data, the information on F_2 is lost. In our calculation we concentrate on the part of Eq. (21) which contains $F_1^V + F_2^V$. The contribution from F_2^V can be determined only when G_M and G_E can be separated from data with better angular resolution.

We take F_M^j in the following form to make a phenomenological fit of the experimental data [10]:

$$F_M^p(t) \sim \frac{x_1}{t^2} + \frac{x_2}{t^3} + \frac{x_3}{t^4} + \frac{x_4}{t^5} + \frac{x_5}{t^6} \ln \frac{t}{Q_0^2}; \quad (27)$$

and

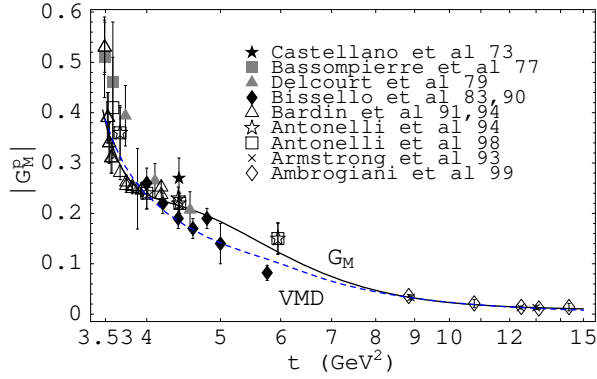


FIG. 3. T in e -like proton magnetic form factor data, fitted (solid) by Eq. (27) with the parameters given in Eq. (29). The other (dashed) curve is discussed in Sec. IV.

$$\mathcal{F}_M^n(t) = \frac{Y_1}{t^2} + \frac{Y_2}{t^3} \ln \frac{t}{Q_0^2}; \quad (28)$$

where the leading power and the logarithmic factor are suggested by PQCD, and the fewer t parameters for G_M^n reflects the fact of scarcer neutron data. We find the best t values

$$\begin{aligned} x_1 &= 429.88 \text{ GeV}^4; & x_4 &= 448583.96 \text{ GeV}^{10}; \\ x_2 &= 10783.69 \text{ GeV}^6; & x_5 &= 635695.29 \text{ GeV}^{12}; \\ x_3 &= 109738.41 \text{ GeV}^8; \end{aligned} \quad (29)$$

and

$$Y_1 = 236.69 \text{ GeV}^4; \quad Y_2 = 579.51 \text{ GeV}^6; \quad (30)$$

where the χ^2 per degree of freedom of the fits are 1.39, 0.41 for \mathcal{F}_M^p and \mathcal{F}_M^n respectively. We show in Figs. 3 and 4 the fitted data together with the best fit curves given by Eq. (27) and Eq. (28) with the parameters above.

It was pointed out in Ref. [8] that the data supports $\mathcal{F}_E^n = 0$ as well. We therefore perform the fit for the neutron magnetic form factor to the data that is extracted under the assumption of $\mathcal{F}_E^n = 0$. Since the number of data points is small, a two-parameter fit as in Eq. (28) would still suffice. The best fit values are

$$Y_1 = 292.62 \text{ GeV}^4; \quad Y_2 = 735.73 \text{ GeV}^6; \quad (31)$$

giving $\chi^2/\text{d.o.f.} = 0.39$ which is a little smaller than the previous fit. To the eye, the data might slightly prefer the second fit, especially the $t = 6 \text{ GeV}^2$ data point. However, it should be clear that more data is needed to distinguish between these two cases. The long dashed line in Fig. 4 shows the best fit to \mathcal{F}_M^n as extracted from data by assuming $\mathcal{F}_E^n = 0$.

We note that there is a sign difference between G_M^p and G_M^n in the space-like region, since from Eq. (18) $G_M^p(0) = 1 + \mu_p > 0$ and $G_M^n(0) = -\mu_n < 0$: Analyticity implies continuity at infinity between space-like and

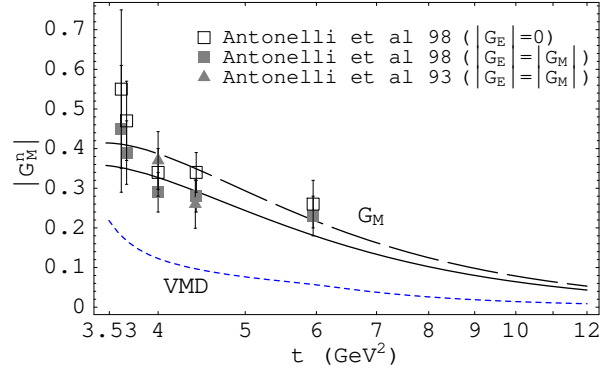


FIG. 4. T in e -like neutron magnetic form factor, where solid (long dashed) line is fitted by Eq. (28) with parameters given in Eq. (30) (Eq. (31)), for data extracted with $\mathcal{F}_E = \mathcal{F}_M$ ($\mathcal{F}_E = 0$) assumption. The third (dashed) curve is discussed in Sec. IV.

time-like t [22] regions. Hence time-like magnetic form factors are expected to behave like space-like magnetic form factors, i.e. real and positive for the proton, but negative for the neutron.

For large t , QCD predicts the magnetic form factors to be real [21], with the neutron form factor weaker than the proton case [23]. According to QCD sum rules [24], asymptotically one expects $G_M^n = G_M^p$, $Q_d = Q_u = 0.5$: We can readily check our fits against these: for G_M^n

fitted to data extracted by assuming $\mathcal{F}_E = \mathcal{F}_M$ for both neutron and proton magnetic form factors, we have $G_M^n = G_M^p = Y_1/x_1 = 236.69/429.88 = 0.55 \approx 0.5$. For G_M^n fitted to the proton data extracted with the assumption $\mathcal{F}_E = \mathcal{F}_M$ but the neutron data extracted assuming $\mathcal{F}_E = 0$, we have $G_M^n = G_M^p = Y_1/x_1 = 292.62/429.88 = 0.68$; slightly larger than 0.5. Nucleon form factors have also been analyzed from negative to positive t with dispersion relations. The phase of the proton magnetic form factor turns out to be $\pi/2$, hence the proton magnetic form factor is real and positive as expected asymptotically, but already from $t \approx 4 \text{ GeV}^2$ [25,26] onwards.

C. Results for $B^0 \rightarrow D^+ \pi^-$

Before using data and the form factor relations to compute the decay rate, we need to specify the value of a_1 to be used. As we will see in the next section, the em current can be seen as coupled to the nucleons by means of vector mesons. Since it is the isovector portion of the em current that is needed, the best value for a_1 would be the one that is extracted from the two-body mode $B^0 \rightarrow D^+ \pi^-$, which gives [18] $a_1^{LF} = 0.74 \pm 0.18 \pm 0.06$ for the light-front form factors and $a_1^{BSW} = 0.86 \pm 0.21 \pm 0.07$ for the BSW form factors.

For both proton and neutron data extracted by assuming $\mathcal{F}_E^j = \mathcal{F}_M^j$, the predicted branching ratios are

$$B_{\Gamma_V}^{LF} = (7.19_{1.09}^{+1.24}) \cdot 10^{-4} \frac{a_1^2}{0.74}; \quad (32)$$

for the light-front (LF) model, and

$$B_{\Gamma_V}^{BSW} = (8.78_{1.34}^{+1.54}) \cdot 10^{-4} \frac{a_1^2}{0.86}; \quad (33)$$

for the BSW model. The subscript V serves as a reminder that this is the result from the vector portion of the weak current alone. The upper and lower bounds correspond respectively to the maximum and minimum of the branching fraction evaluated by scanning through both $2_{\min}^2 + 1$ of \mathcal{F}_M^p and \mathcal{F}_M^n fits.

For proton data extracted by assuming $\mathcal{F}_E^p = \mathcal{F}_M^p$ but neutron data extracted by assuming $\mathcal{F}_E^n = 0$, we have

$$B_{\Gamma_V}^{LF} = (9.01_{1.58}^{+1.83}) \cdot 10^{-4} \frac{a_1^2}{0.74}; \quad (34)$$

$$B_{\Gamma_V}^{BSW} = (11.01_{1.96}^{+2.26}) \cdot 10^{-4} \frac{a_1^2}{0.86}; \quad (35)$$

The larger values for this second set of branching fractions can be understood qualitatively from Fig. 4, where the curve fitted to data assuming $\mathcal{F}_E^j = 0$ is higher than the one fitted assuming $\mathcal{F}_E^j = \mathcal{F}_M^j$. Since the neutron magnetic form factor is negative in the time-like region, the quantity $G_M^p - G_M^n$ is larger if G_M^n gets more negative, and the branching fraction becomes larger.

Comparing with the central value of the measured $\text{Br}(B^0 \rightarrow D^+ p n) = (14.5_{3.0}^{+3.4} \cdot 2.7) \cdot 10^{-4}$, our LF (BSW) model results contribute 50 (61)% for the first set and 62 (76)% for the second. If the naive factorization value for a_1 is used, the light-front results are close to the experimental central value, that is $B_{\Gamma_V}^{LF(BSW)} = 13.93 (12.59) \cdot 10^{-4}$ for the first set and $17.46 (15.79) \cdot 10^{-4}$ for the second set. Fig. 5 shows the vector current induced differential decay rate $d\Gamma_V/dt = d\Gamma/dq^2$, for both the light-front and the BSW models. The lower two curves are from the approach of next section. As we have seen in Eqs. (32)-(35), the LF form factor model gives results that are smaller than the BSW model case. The 10% difference can be viewed as an estimate of the uncertainty from b.c. form factors.

From Fig. 5 we see that the differential rate peaks at 4.3 GeV^2 , corresponding to $m_{pn} \approx 2.07 \text{ GeV}$, which is quite close to the threshold of 1.88 GeV . This threshold enhancement effect, as suggested in Ref. [4], should be checked experimentally by measuring the recoil D momentum spectrum.

Although the time-like data for the form factors of the axial current is still lacking, we can nevertheless make a rough estimate of the contribution from the axial current. In analogy with the nucleon em form factors which

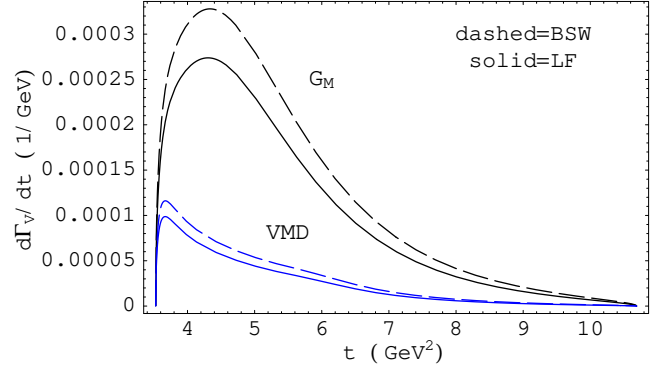


FIG. 5. The differential decay rate of the vector current induced $B^0 \rightarrow D^+ p n$ decay vs $t = m_{pn}^2$. The upper two curves are from the phenomenological fits to nucleon form factor data assuming $\mathcal{F}_E^j = \mathcal{F}_M^j$ for the Light-Front (solid) and BSW (dash) models for $B^0 \rightarrow D^+$ form factor. The lower two curves are from the VMD-based nucleon form factor model discussed in the next section.

are constrained by the asymptotic form of Eq. (25), we expect that, for large t , $g_A(t)$ behaves as $1/t^2$ and dominates over $h_A(t)$, which behaves like $1/t^3$. The assumed smallness of the h_A contribution is supported by the exchange contribution being negligible as discussed in the previous section. Taking cue from the similarity between Eqs. (21) and (23), we estimate the axial vector contribution by making a simple comparison and scaling from the vector case. Since we only have space-like information for the $g_A(t)$ form factor, we estimate $g_A(t_{th})$ at threshold by assuming same threshold enhancement factor as the $G_M^p(t) - G_M^n(t)$ case.

With this and Eqs. (21) and (23) in mind, to estimate the axial vector current contribution, we scale the decay rate obtained from the vector case by the ratio $g_A^2(t_{th}) = (G_M^p(t_{th}) - G_M^n(t_{th}))^2$ for space-like momentum. We use a dipole fit $g_A(t) = g_A(0) = (1 - t/M_A^2)^2$ with the axial mass $M_A = 1.077 - 0.039 \text{ GeV}$ [27]. For $t = 4m_N^2$, the ratio $r(t) = g_A(t) = (G^p(t) - G_M^n(t))$ gives $r(4m_N^2) \approx 0.59$. Assuming this ratio holds also at the threshold $t = 4m_N^2$, then $r^2(4m_N^2) \approx 0.35$ could be taken as the ratio of the branching fraction from the weak axial vector current to that from the weak vector current, i.e. $B_{\Gamma_A} = B_{\Gamma_V} \cdot r^2(4m_N^2)$. For the results from fitting data assuming $\mathcal{F}_E^j = \mathcal{F}_M^j$, the total rate $\text{Br} = B_{\Gamma_V} + B_{\Gamma_A}$ would then be $B_{\Gamma_V}^{LF} (1 + 0.35) = (7.19 \cdot 10^{-4}) = 9.71 \cdot 10^{-4}$ and $B_{\Gamma_V}^{BSW} 11.85 \cdot 10^{-4}$. On the other hand, for the results from fitting data assuming $\mathcal{F}_E^j = 0$, the total rate would be $B_{\Gamma_V}^{LF} (1 + 0.35) = (9.01 \cdot 10^{-4}) = 12.16 \cdot 10^{-4}$ and $B_{\Gamma_V}^{BSW} 14.86 \cdot 10^{-4}$, quite compatible with the experimental value of $(14.5_{3.0}^{+3.4} \cdot 2.7) \cdot 10^{-4}$. Another value of t which could be of interest is $t = 0$. Assuming that the ratio $r(0) \approx 0.27$ holds at threshold, then from $r^2(0) \approx 0.07$, $B_{\Gamma_A} = B_{\Gamma_V} \cdot r^2(0)$, the total rate $\text{Br} = B_{\Gamma_V} + B_{\Gamma_A}$

is dominated by the vector current contribution. To improve our result, we urge for more experimental measurements on $G_M^N(t)$; $G_E^{p,n}(t)$ and $g_A(t)$.

IV. VECTOR-MESON-DOMINANCE APPROACH

The pole model of Sec. II that used ρ^+ as intermediate particle in Eq. (5) can be linked to the factorization approach in Sec. III by the following substitution

$$\frac{P}{2F_i^v} \rightarrow \frac{m_f g_i^{NN}}{m^2 - t}; \quad (36)$$

in Eq. (21). The denominator in the above substitution arises from the ρ^+ propagator, m_f from the creation of ρ^+ and g_i^{NN} is from the ρ^+ -nucleon coupling constant. Among the various approaches to the nucleon form factors, of particular interest is the Vector-Meson-Dominance (VMD) hypothesis, which states that a photon couples to the hadrons via intermediate vector mesons such as ρ , ω , ϕ , etc. The simple pole model of Sec. II is a limited form of the VMD hypothesis. In Ref. [28], a parameterization of the nucleon form factors based on dispersion analysis was proposed, which is constrained by several physical conditions, including PQCD power counting. We shall briefly describe this approach in what follows, as one could gain some insight.

A. Dispersion Analysis and VMD Hypothesis

In the VMD approach, starting from the dispersion relation

$$F(t) = \frac{1}{t_0} \int_{t_0}^{\infty} \frac{\text{Im} F(t')}{t' - t} dt'; \quad (37)$$

where $F(t)$ stands for the nucleon form factors $F_{1,2}^v(t)$, one approximates the spectral functions by a few vector meson poles. Thus, the form factors take the form

$$F_i^v(t) = \sum_v \frac{a_i^v}{M_v^2 - t}; \quad i=1,2; \quad (38)$$

where $a_{1,2}^v$ are related to the vector ($i=1$) and tensor ($i=2$) coupling constants via

$$\frac{P}{2a_i^v} = m_v f_v g_i^{vNN}; \quad (39)$$

and f_v is the vector meson decay constant. This clearly extends the simple meson exchange case of Eq. (36), where we show the Feynman diagram in Fig. 6.

Following Ref. [28] we now consider the following parameterization of the form factors:

$$F_i^v(t) = F_i^v(t) + \sum_v \frac{a_i^v L^{-1}(M_v^2)}{M_v^2 - t} L(t); \quad (40)$$

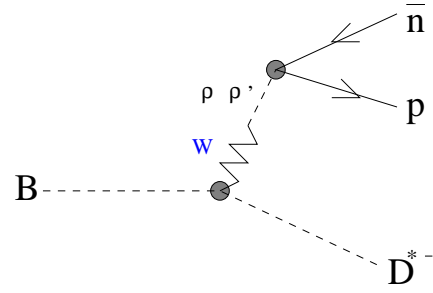


FIG. 6. The Feynman diagram for the VMD approach. The W boson couples to the nucleon pair via vector mesons which in our case are ρ and three excited states. Only ρ and the first excited state is shown.

where

$$L(t) = \ln \frac{2}{Q_1^2 - t}; \quad (41)$$

$$F_i^v(t) = \frac{a_i L^{-1}(M_a^2) + b_i L^{-1}(M_b^2) + c_i t^{-d_i}}{2 - d_i}; \quad (42)$$

for $i=1,2$, where $a_1 = 1.0317$, $a_2 = 5.7824$, $b_1 = 0.0875$, $b_2 = 0.3907$, $c_1 = 0.3176$, $c_2 = 0.1422$, $d_1 = 0.5496$, $d_2 = 0.5362$, and $M_a^2 = 0.5 \text{ GeV}^2$, $M_b^2 = 0.4 \text{ GeV}^2$.

Since the form factors also receive constraints from perturbative QCD for large momentum transfer as explained in the previous section, a logarithmic factor of the form in Eq. (41) is given to be consistent. It can easily be seen that the form of Eq. (40), apart from the logarithmic factor, contains contributions from two terms: one given by $F_i^v(t)$ which represents the 2^{-1} continuum including that from ρ , the other given by the summation which represents the VMD approach of additional isovector vector meson poles. The coefficients a_i^v in the summation represent the combination given in Eq. (39).

In Ref. [28] where the space-like nucleon form factors are fitted, it was found sufficient to use 3 additional vector meson poles, two of which are chosen to be the physical particles ($\rho(1450)$ and $\rho(1700)$). In Ref. [26] which extends the scenario to include time-like data, the third pole is left adjustable to compensate for the neglect of higher mass continua like $N\bar{N}$. It was determined to be $M_v = 1.4035 \text{ GeV}$ in association with $t^2 = 12 \text{ GeV}^2$ and $Q_1^2 = 0.35 \text{ GeV}^2$. The parameters in Eq. (42) remain unaffected in both fits.

Note that all the above are just fixing the positions of the poles or, in other words, fixing the identities of the vector mesons taking part in the VMD approach. Due to our insufficient understanding of the quantities other than the masses in a_i^v , other constraints are still needed to completely specify these coefficients. This is in contrast with the $\rho(770)$ pole about which we know much

more. It is thus isolated from the summation so that $F_i(t)$ contains no parameters that need to be determined.

Among the several distinct constraints given in Ref. [28], one of which concerns the asymptotic form of Eq. (25). It can be achieved by choosing the residues a_i^V of the vector meson pole terms such that the leading coefficients in the $1-t$ expansion cancel. This is what the use of a single ρ -pole can never achieve, since further excited states are needed for the cancellation. By making use of the isospin relation between the weak vector current and the isovector portion of the em current and the VMD assumption, the W boson can now be seen to couple to the nucleon pair via the vector mesons which in this analysis are ρ^+ and three of its higher excited states.

After implementing all the constraints including the asymptotic form, the specification of the coefficients in the VMD approach is then complete. The logarithmic factor in Eq. (25) is approached by $L(t)$ of Eq. (41). We summarize in Table II the relevant meson poles and the corresponding residues of the higher excited states given by Table 1 of Ref. [26] (only the so-called $\rho(1700)$ is needed).

B. Results from VMD Approach

The parametrization agrees with experiment quite well [29] up to $t \approx 6 \text{ GeV}^2$, beyond which it overruns data because of the logarithmic factor $L(t)$. This is in contrast with the empirical t of Eq. (26).

In order to conform to experiment for larger momentum transfer, a modification of the logarithmic factor $L(t)$ is needed. The empirical t of Eq. (26) suggests a convenient modification

$$L(t) = \begin{cases} \ln \frac{t}{Q_1^2} & \text{for } t > \frac{t_0}{2} ; \\ \frac{1}{2} L^0 \frac{t}{2} + H(\cdot) & \text{for } \frac{t_0}{2} < t < \frac{t_0}{2} + \frac{t_0}{2} ; \\ \ln \frac{t}{Q_1^2} & \text{for } t < \frac{t_0}{2} + \frac{t_0}{2} ; \end{cases}$$

where we match a parabola between the interval $\frac{t_0}{2} < t < \frac{t_0}{2} + \frac{t_0}{2}$ by tuning the constant $H(\cdot)$. Note that $L^0 \frac{t}{2} = L^0 \frac{t_0}{2} + \frac{t_0}{2}$ and $L^0 \frac{t_0}{2} = L^0 \frac{t_0}{2} + \frac{t_0}{2}$, or $L(t)$ is symmetric with respect to $t = \frac{t_0}{2} + \frac{t_0}{2}$.

TABLE II. The relevant poles (M_v in GeV) and the corresponding residues that enter the summation in Eq. (40).

$M_0 = 1.4035$		$M_\infty = 1.45$		$M_{\infty\infty} = 1.69$	
a_1	a_2	a_1	a_2	a_1	a_2
9.913	4.731	13.01	0.263	3.497	2.947

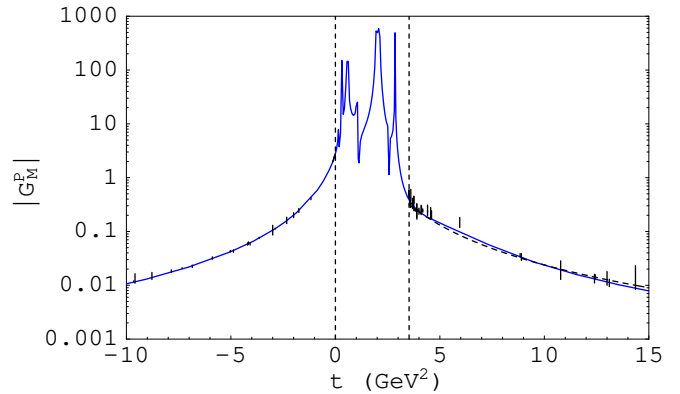


FIG. 7. The VMD-based proton magnetic form factor with the modified logarithmic factor. The dash-line in the time-like region represents a t with $C = 53$ in Eq. (26).

$^2=2$. To smooth out the artificial rise that occurs beyond $t \approx 6 \text{ GeV}^2 = t_0$ for the original t , we choose $H(\cdot) = 0.5 \text{ GeV}^{-2}$ and $H(\cdot) = 0.10279$.

Fig. 7 shows the resulting VMD-based proton magnetic form factor with the modified logarithmic factor in the time-like region. The result is plotted in more detail in Fig. 3 in the time-like region. We see that the trend of the proton data can be described by this model. In contrast, from Fig. 4, where the extension of the VMD result to neutron case is given, there is a significant deviation from G_M^n data, signaling the incapability of the three-plus-one pole t to describe the neutron data consistently. This fact was admitted to in both Ref. [26] and Ref. [30].

Recall that analyticity can help determine the signs of the time-like form factors from space-like region. Unlike Eqs. (27) and (28) where the signs are put in by hand, it is more natural for the dispersion analysis since all the time-like information in principle can be obtained via the dispersion relation in Eq. (37), where the spectral function $\text{Im} F(t)$ is analytically continued from the space-like region. One can readily check this by finding out the value of the magnetic form factors from the VMD analysis at threshold: $G_M^p(4m_N^2) = +0.39$ while $G_M^n(4m_N^2) = -0.22$. From both Figs. 3 and 4, since neither G_M^p nor G_M^n seem to cross the t -axis, G_M^p remains positive while G_M^n remains negative throughout the time-like region. VMD analysis thus gives G_M^p and G_M^n with a relative sign.

With all the em form factors at hand, we can again calculate the branching fraction of $B^0 \rightarrow D^+ \pi^-$ through the vector portion of the charged weak current. We still need to determine the effective coefficient a_1 to be used. We again take a_1 as extracted from fitting $B^0 \rightarrow D^+ \pi^-$. The results for $B^0 \rightarrow D^+ \pi^-$ are,

$$B_{\mathcal{R}_V}^{LF} = (1.69 \cdot 10^4) \frac{a_1}{0.74}{}^2 ; \quad (43)$$

$$B_{\mathcal{R}_V}^{BSW} = (2.06 \cdot 10^4) \frac{a_1}{0.86}{}^2 ; \quad (44)$$

which are respectively about 12% and 14% of the experimental value of $(14.5^{+3.4}_{-3.0} - 2.7) \cdot 10^4$.

Among the three masses given in Table II the results are less sensitive to the variation of the third mass M_{000} for which a change of 1 MeV causes only a 1% variation in branching fractions. A variation of the same magnitude in other pole masses causes nearly 10% change. For variations up to 10 MeV, the smallest variation of the branching fractions is still given by perturbing M_{000} , which causes nearly 10% variation.

From Fig. 5 one sees that the differential decay rate peaks not far above the pn threshold of $t = 3.53 \text{ GeV}^2$. The contributions from the region of $3.53 < t < 6 \text{ GeV}^2$ is more than 80% of the total rate for both LF and BSW models. Had we used the unmodified logarithmic factor of Eq. (41), as a result of the artificial rise characterized by the original logarithmic factor, the contributions from $t > 6 \text{ GeV}^2$ ($m_{pn} > 2.45 \text{ GeV}$) would be nearly 2.5 times higher. The contribution from $t < 6 \text{ GeV}^2$, however, are not affected as mentioned earlier.

We note that the branching fractions obtained in the VMD approach are typically 4 times smaller than those from the phenomenological model of the previous section. This can be understood qualitatively from Fig. 4, where one sees that the absolute value of the neutron form factor in VMD approach stays below all the data points. The VMD model was tuned more on the proton form factor, where data is much more abundant. Analyticity implies that the proton magnetic form factor is positive while the neutron one remains negative throughout the time-like region. Hence, $G_M^p - G_M^n$ would be larger for more negative G_M^n values. So, if G_M^n in VMD approach moves upward to meet the data, the combination $G_M^p - G_M^n$ would increase and the result would rise accordingly. We illustrate the point further in Fig. 8, where the dotted line represents $G_M^p - G_M^n = 2(F_1^v + F_2^v)$ from

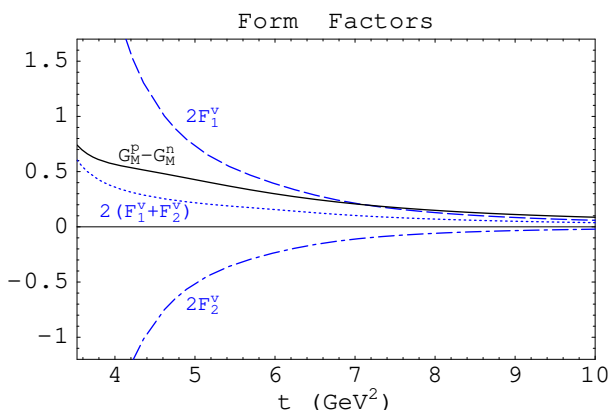


FIG. 8. $G_M^p - G_M^n$ (solid) from our t to nucleon form factor data compared with $2F_1^v + 2F_2^v = G_M^p - G_M^n$ (dotted) from the VMD analysis, for the kinematically allowed region of t in $B^0 \rightarrow D^0 pn$. Also shown are $2F_1^v$ (dashed) and $2F_2^v$ (dot-dashed) from the VMD model.

the VMD model, which stays below the phenomenological fit of nucleon form factors, denoted by solid line.

An improved VMD model that gives a better account of the time-like data, especially for G_M^n , will give a better agreement to the result of the previous section.

V. DISCUSSION AND APPLICATIONS

A. Nucleon Form Factor Decompositions

One advantage of the VMD approach is that it not only gives G_M^{pn} but also the F_2 form factor as well. It is useful then to check contributions from each parts in the model. The amplitude from the weak vector current in Eq. (21), upon squaring, can be expressed as

$$\mathcal{M}_{Vj}^2 = \mathcal{M}_{F_1+F_2}^2 + \mathcal{M}_{F_2}^2 + 2\text{Re} \mathcal{M}_{F_1+F_2} \mathcal{M}_{F_2} \quad (45)$$

with $\mathcal{M}_{F_1+F_2;F_2}$ denoting $F_1^v + F_2^v; F_2^v$ terms in Eq. (21). We decompose the branching fraction as $B_{F_1} = B_{F_1+F_2} + B_{F_2} + B_{(F_1+F_2)F_2}$ where the last term is the interference term. The ratio $R_{(F_1+F_2)} = B_{(F_1+F_2)F_2} / B_{(F_1+F_2)}$ measures the fraction from the $(F_1^v + F_2^v)$ alone, and likewise for R_{F_2} and $R_{(F_1+F_2)F_2}$. We find $R_{(F_1+F_2)}; R_{F_2}; R_{(F_1+F_2)F_2}$ 130%; 24%; 54% in the VMD model. Note that the $2(F_1^v + F_2^v) = G_M^p - G_M^n$ term gives the dominant contribution, which supports the approximation used in the previous section. The F_2^v contribution is much smaller even though $|F_2^v(t)|$ is greater than $|F_1^v + F_2^v|$ for $t < 5 \text{ GeV}^2$, as shown in Fig. 8. The interference term contributes 40% with respect to $F_1^v + F_2^v$ contribution. The destructive nature is traced back to the opposite sign between $F_1^v + F_2^v$ and F_2^v as shown in Fig. 8. This destructive interference leads to a further reduction of the contribution from the last two terms in Eq. (45).

It is instructive to compare with Eq. (12), where one decomposes into F_1 and F_2 directly. As we show in Table III, the individual terms from this decomposition are all an order of magnitude larger, and one relies on strong cancellations to maintain B_{F_1} . It is therefore not a very useful decomposition. We see from Fig. 8 that the magnitudes of F_1^v and F_2^v are all greater than their sum, hence

TABLE III. Comparison of nucleon form factor decompositions. The fraction $R_X = B_X / B_{F_1}$ are defined in text, where X stands for any combination of F_1, F_2 or their product.

	$R_{(F_1^v + F_2^v)}$	$R_{F_2^v}$	$R_{(F_1^v + F_2^v)F_2^v}$
LF (BSW)	1.3	0.24	0.54
	$R_{F_1^v}$	$R_{F_2^v}$	$R_{F_1^v F_2^v}$
LF (BSW)	26.00	18.25	43.25

$F_1^V + F_2^V$ together with F_2^V is a better decomposition for t close to threshold.

Recall that in the previous section we started with the assumption of color transparency of the nucleon pair. By an isospin relation among the weak vector and em currents, the VMD picture can also be applied in the three body decay case. The weak current produces vector mesons first, which are certainly lighter and less complicated objects compared with the baryon pair. Since the factorization approach gives reasonable result on $B^0 \rightarrow D^+ \bar{p}n$ with 20{30% nonfactorizable effect, the color transparency of the nucleon pair is validated to some extent. Furthermore, the only difference between the naive pole model discussed in Section II and the VMD model is that here we need not only but also its higher excited states to give better consistency to QCD asymptotic behavior of form factors, which can be viewed as a form of quark-hadron duality. This duality may also serve as an explanation for the threshold enhancement which is critical to give large three body decay rate for soft baryon pairs.

B. Predictions for $B \rightarrow D^{(*)}pn$ Modes

Our phenomenological approach can be applied to the modes of $B^+ \rightarrow D^{(*)}pn$ and $B^0 \rightarrow D^{(*)}pn$. We show in Table IV the results based on the vector current with the $B^0 \rightarrow D^{(*)}pn$ mode included for comparison. We have used the central values of the effective coefficients that are extracted from the two-body modes [18] $B^0 \rightarrow D^+ \bar{p}, D^+ \bar{n}$ with values $a_1^{LF(BSW)} = 0.74 \pm 0.18 \pm 0.06$ ($0.86 \pm 0.21 \pm 0.07$) and $a_1^{LF(BSW)} = 0.89 \pm 0.08 \pm 0.07$ ($0.91 \pm 0.08 \pm 0.07$) respectively. We note that the D modes in Table IV are close in rate, and likewise for D modes, which is easy to understand because of similarity in decay amplitude. In Fig. 9 we show the differential decay rates arising from the vector current for the other three $B \rightarrow D^{(*)}pn$ decays.

Although only the contribution from the weak vector current can so far be calculated, we can estimate the

TABLE IV. Branching fractions of the $B \rightarrow D^{(*)}pn$ modes from the vector current, obtained by using the phenomenological form factors with $\mathcal{F}_M^n(j) = \mathcal{F}_E^V(j)$ but $\mathcal{F}_M^n(j) = \mathcal{F}_E^n(j)$ for the first set and $\mathcal{F}_E^n(j) = 0$ for the second set of B rs.

	$B_{rv} \cdot 10^4$		$B_{rv} \cdot 10^4$	
	$\mathcal{F}_M^n(j) = \mathcal{F}_E^n(j)$		$\mathcal{F}_E^n(j) = 0$	
	LF	BSW	LF	BSW
$B^0 \rightarrow D^+ \bar{p}n$	$7.19^{+1.24}_{-1.09}$	$8.78^{+1.54}_{-1.34}$	$9.01^{+1.83}_{-1.58}$	$11.01^{+2.26}_{-1.96}$
$B^+ \rightarrow D^0 \bar{p}n$	$7.69^{+1.33}_{-1.33}$	$9.39^{+1.65}_{-1.44}$	$9.65^{+1.95}_{-1.69}$	$11.79^{+2.42}_{-2.10}$
$B^+ \rightarrow D^0 \bar{p}n$	$3.95^{+0.59}_{-0.53}$	$3.23^{+0.46}_{-0.42}$	$4.93^{+0.87}_{-0.77}$	$4.03^{+0.69}_{-0.61}$
$B^0 \rightarrow D^+ \bar{p}n$	$3.69^{+0.55}_{-0.49}$	$3.02^{+0.43}_{-0.43}$	$4.60^{+0.81}_{-0.72}$	$3.76^{+0.64}_{-0.57}$

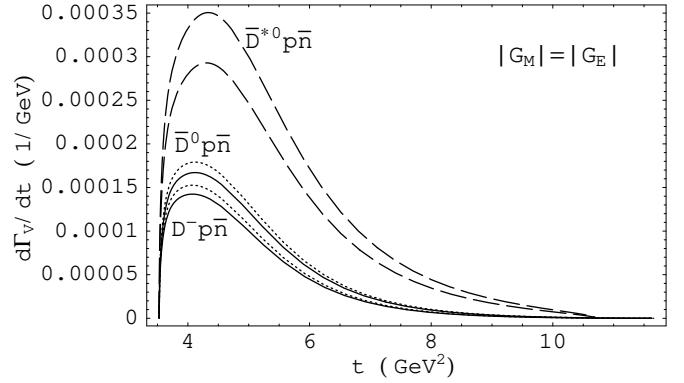


FIG. 9. The differential decay rates arising from nucleon vector current. Upper (lower) dashed line is for $B^0 \rightarrow D^0 p \bar{n}$ with the BSW (LF) hadronic form factors; upper (lower) dotted and solid lines are for the $B^0 \rightarrow D^0 p \bar{n}$ and $B^0 \rightarrow D^- p \bar{n}$ modes using the LF (BSW) model.

values of these other baryonic modes by following the recipe of Sec. III. Table V shows the predicted branching fractions that would emerge experimentally for $B^+ \rightarrow D^0 p \bar{n}, B^+ \rightarrow D^0 p \bar{n}$ and $B^0 \rightarrow D^- p \bar{n}$. Note that $B^+ \rightarrow D^0 p \bar{n}$ is predicted at $15.5 \cdot 10^{-4}$ and is only slightly larger than the $B^0 \rightarrow D^- p \bar{n}$ mode. The rates of the other two modes are only 2{3 times smaller.

One can see from both Tables IV and V as well as Fig. 9 that the LF results are generally greater than the BSW ones for $B \rightarrow D$ modes, but the case is reversed for the $B \rightarrow D$ modes. This can be understood from the differences in a_1 and hadronic form factors of the LF and BSW cases. For the $B \rightarrow D$ modes, the only hadronic form factor involved is $F_1^{B,D}$, which behaves as a dipole and monopole in the LF and BSW models, respectively. This leads to $F_1^{LF}(t) > F_1^{BSW}(t)$ in the physical timelike region while $a_1^{LF} = a_1^{BSW} = 0.9$, giving a larger B_{rv}^{LF} . In contrast, for $B \rightarrow D$ modes, although the dominant hadronic form factor $A_1^{LF} > A_1^{BSW}$ in the physical timelike region, it behaves as monopole for both LF and BSW models, hence the difference between A_1^{LF} and A_1^{BSW} is not as large as the previous case. However, $a_1^{LF} = 0.74 < a_1^{BSW} = 0.86$ hence we have the opposite

TABLE V. Estimated Branching fractions via $Br = 14.5 \cdot 10^{-4} \cdot B_{rv} \cdot B \rightarrow D^{(*)}pn = Br_{rv} \cdot B^0 \rightarrow D^{(*)}pn$ where $14.5 \cdot 10^{-4}$ is the central value of Eq. (1)

	$Br \cdot 10^4$		$Br \cdot 10^4$	
	$\mathcal{F}_M^n(j) = \mathcal{F}_E^n(j)$		$\mathcal{F}_E^n(j) = 0$	
	LF	BSW	LF	BSW
$B^+ \rightarrow D^0 \bar{p}n$	15.51	15.51	15.53	15.93
$B^+ \rightarrow D^0 \bar{p}n$	7.97	5.33	7.93	5.31
$B^0 \rightarrow D^- p \bar{n}$	7.44	4.99	7.40	4.95

TABLE VI. Branching fractions for $B^0 \rightarrow D + \text{Strange Baryons}$ from vector current using the phenomenological G_M form factors of Sec. III, and by using the VMD model.

		$Br_V^{LF} \cdot 10^4$		$Br_V^{BSW} \cdot 10^4$	
		G_M	VMD	G_M	VMD
$B^0 \rightarrow D$	pn	7.19	1.69	8.78	2.06
$B^0 \rightarrow D$	$^+$	0.51	0.11	0.65	0.14
$B^0 \rightarrow D$		0.50	0.11	0.63	0.14
$B^0 \rightarrow D$	$^0^+$	0.31	0.07	0.40	0.09
$B^0 \rightarrow D$	0	0.30	0.07	0.38	0.08
$B^0 \rightarrow D$	0	0.04	0.01	0.06	0.01

result that BSW rates are bigger.

C. Predictions for $B^0 \rightarrow D + \text{Strange Baryons}$

Our phenomenological approach as well as the VMD-based analysis can be extended to B^0 decay into D plus baryon pairs containing strangeness. In Table VI we list the results of strange baryonic pairs in comparison with pn. For the phenomenological G_M approach, we only show the $\mathcal{F}_M^n(j) = \mathcal{F}_M^n(j)$ case. The strange baryon modes all have rates smaller than that of the pn mode due to the following reasons.

First, the coefficients arising from SU(3) rotations [31] of the pn-state to other states suppress the couplings between the meson and the baryons, as shown in the second column of Table VII. Second, since the form factors are monotonically decreasing functions of the momentum transfer, as shown in Fig. 8, the higher thresholds further reduce the rate. In Table VII, we estimate this reduction as scaling by $(1-t^2)^2$ in rate. Estimates are close to R which is obtained by using Eq. (21).

As a result of threshold effects, the lightest mass pair $^+$ should be the largest in rate. Furthermore, since charge-conjugate states have the same meson-baryon couplings, the only difference between the charge-conjugate rates must solely come from the mass difference of the baryons, which is usually small. On the other hand, the heaviest 0 has the smallest rate.

In Fig. 10 we show the differential decay rates for $B^0 \rightarrow D^+, D^{+0}$ and D^0 with the LF hadronic form factors. These modes can be distinguished in the plot by their thresholds. There are two sets of curves standing for the phenomenological and VMD models respectively.

By following the same method in obtaining the results of Table V, we estimate and show the expected branching fractions of the strange modes in Table VIII. The largest modes are $B^0 \rightarrow D^+, D^{+0}$, and D^0 , which are an order of magnitude below the nucleon pair mode. It is also worth mentioning that we can extract baryon spin information by the self-analyzing power of 0 -decay

TABLE VII. Estimated ratios of rates for strangeness modes to pn mode as described in text. Values in the last column are obtained from Br_V^{LF} with VMD-based analysis, where $a = (g^{B_s B_s} = g^{pn})^2$ and $b = (m_p + m_n)^8 = (m_{B_s} + m_{B_s})^8$.

$B_s B_s$	a	b	a/b	R
$^+$	0.287	0.192	0.055	0.067
$^+^0$	0.287	0.192	0.055	0.067
$^0^+$	0.236	0.152	0.036	0.043
0	0.236	0.147	0.035	0.040
0	0.097	0.066	0.006	0.005

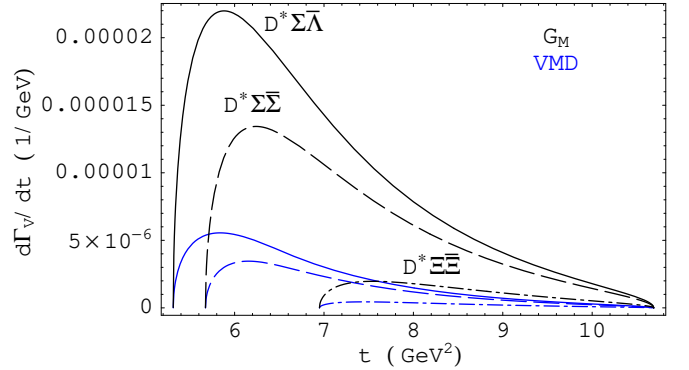


FIG. 10. Differential rates of $B^0 \rightarrow D^+ +$ (solid), D^{+0} (dashed) and D^0 (dot-dashed), with LF hadronic form factors. The two sets of curves stand for the phenomenological (upper) and VMD models respectively.

in these modes, the spin information may be useful to construct CP-observables [4].

VI. CONCLUSION

We presented in this paper three different approaches to account for CLEO's result on $B^0 \rightarrow D + pn$: a sim-

TABLE VIII. Estimates for $Br(B^0 \rightarrow D B_s B_s)$ based on Table VI following the same way as in Table V. G_M denotes the phenomenological form factor model constructed in Sec. III, and the other is for the VMD model.

		$Br_V^{LF} \cdot 10^4$		$Br_V^{BSW} \cdot 10^4$	
		G_M	VMD	G_M	VMD
$B^0 \rightarrow D$	$^+$	1.04	0.95	1.07	0.98
$B^0 \rightarrow D$		1.00	0.92	1.04	0.95
$B^0 \rightarrow D$	$^0^+$	0.63	0.58	0.65	0.60
$B^0 \rightarrow D$	0	0.61	0.56	0.63	0.58
$B^0 \rightarrow D$	0	0.09	0.07	0.09	0.08

ple pole model, a factorization approach based on nucleon form factor data, and a VMD approach. The pole model is intuitively clear, however, not reliable due to our ignorance of the strong interaction. In the factorization approach where we assume color transparency of the nucleon pair, the pair is viewed as produced directly from the weak current. We then capitalize on an isospin relation of weak and em vector currents to obtain the vector weak nucleon form factors directly from their em partners, where a relatively large database exists. Interestingly, we can account for 60% of the observed $\text{Br}(B^0 \rightarrow D^+ \text{pn})$ rate in this way. To link these two approaches together, we resort to a VMD approach that extends the pole model picture, but at the same time attempts at fitting nucleon form factor data. This approach helps provide insight to the proximity of the three body mode and $B^0 \rightarrow D^+ \text{pn}$, as well as the assumption of color transparency of the factorization approach.

Interference of the weak vector current induced amplitude with the amplitude induced by the weak axial current does not manifest itself in the total rate. The latter is a simple sum of the absolute squares of both vector and axial vector. A rough estimate of axial vector contribution, together with the dominant vector contribution, seem to fit the measured rate. However, for a more reliable calculation, more measurements on timelike region $G_E^{p;n}$ and g_A are urged.

We apply our analysis to $B^+ \rightarrow D^{(*)0} \text{pn}$ and $B^0 \rightarrow D^+ \text{pn}$ modes to get the rates arising from the vector current. Because of the similarity between D^+ and D^0 , $\text{Br}_{\text{V}}(B^+ \rightarrow D^0 \text{pn}) \approx \text{Br}_{\text{V}}(B^0 \rightarrow D^+ \text{pn})$ are comparable in rate. Similarly, we have $\text{Br}_{\text{V}}(B^+ \rightarrow D^0 \text{pn}) \approx \text{Br}_{\text{V}}(B^0 \rightarrow D^+ \text{pn})$. Largely because of the difference between a_1^{LF} and a_1^{BSW} , the LF results are generally bigger than the BSW ones in $B^+ \rightarrow D^0 \text{pn}$ modes while one has the opposite in $B^+ \rightarrow D^+ \text{pn}$ modes. We therefore predict $B^+ \rightarrow D^0 \text{pn}$ to have rate comparable to that of $B^0 \rightarrow D^+ \text{pn}$. The $B^+ \rightarrow D^+ \text{pn}$ modes have smaller rates at the level of 10^{-4} .

Our analysis is also applied to baryonic modes that contain strangeness. The estimated branching fractions are generally lower than the pn mode due to smaller couplings and higher thresholds. The largest modes, $B^0 \rightarrow D^+ \text{pn}$ and D^+ , are predicted to be at the level of 10^{-4} .

For the analogous picture of $B^+ \rightarrow D^0 \text{p}; \text{pn}$ as descending from $B^+ \rightarrow D^0 \text{K}$ and K via $K^{(*)}$ exchange, the baryon pairs are not produced by the W boson, and it seems that the approach used here cannot be readily applied. However, some experience obtained may still be valuable. For example, in the VMD approach to $B^+ \rightarrow D^+ \text{pn}$, more than one pole and cancellations among them are required to reproduce the QCD predicted asymptotic behavior. For the charmless cases, the baryon pairs are no longer produced by the charged current. Instead, the $K^{(*)}$ resonances that correspond to $G_{0;0}^{\text{K}^0;K^0}$ in VMD approach, appear more as string excita-

tions. They need not obey the same QCD power countings, and perhaps may result in larger rates.

Finally, it is of great interest to estimate the rate of the charmless baryonic mode $B^0 \rightarrow D^+ \text{pn}$ by replacing D^+ in the Feynman diagram depicted in Fig. 2 with D^0 . Since this is a tree-dominant mode, extending from the study presented in this paper, $\text{Br}(B^0 \rightarrow D^+ \text{pn})$ could be as large as that of the two-body mode $B^0 \rightarrow D^+ \text{pn}$, analogous to the relative strength of $\text{Br}(B^0 \rightarrow D^+ \text{pn})$ vs $\text{Br}(B^0 \rightarrow D^+ \text{pn})$. Estimating via $\text{Br}(B^0 \rightarrow D^+ \text{pn}) \approx \text{Br}(B^0 \rightarrow D^+ \text{pn}) \approx \text{Br}(B^0 \rightarrow D^+ \text{pn})$. From $\text{Br}(B^0 \rightarrow D^+ \text{pn}) \approx 20(40) \times 10^{-6}$ [12,32] we get $\text{Br}(B^0 \rightarrow D^+ \text{pn}) \approx (0.4(0.8)) \times 10^{-5}$. Alternatively, we can scale from $B^+ \rightarrow D^+ \text{pn}$ by $\int V_{ub} = V_{cb}^2$ and phase space, decay constant etc., and again find $B^+ \rightarrow D^+ \text{pn}$ at 10^{-5} order. Charmless decays are of great current interest. A more detailed discussion of $B^+ \rightarrow D^+ \text{pn}$ modes are given elsewhere.

ACKNOWLEDGMENTS

We thank S. J. Brodsky for illuminating discussions and useful suggestions. This work is supported in part by the National Science Council of R.O.C. under Grants NSC-89-2112-M-002-063, NSC-89-2811-M-002-0086 and NSC-89-2112-M-002-062, the MOE CosPA Project, and the BCP Topical Program of NCTS.

-
- [1] I. Dunietz, Phys. Rev. D 58, 094010 (1998) [hep-ph/9805287].
 - [2] S. Anderson et al. [CLEO Collaboration], Phys. Rev. Lett. 86, 2732 (2001) [hep-ex/0009011].
 - [3] D. E. Groom et al. [Particle Data Group Collaboration], Eur. Phys. J. C 15, 1 (2000).
 - [4] W. S. Hou and A. Soni, Phys. Rev. Lett. 86, 4247 (2001) [hep-ph/0008079].
 - [5] T. E. Browder et al. [CLEO Collaboration], Phys. Rev. Lett. 81, 1786 (1998) [hep-ex/9804018].
 - [6] C. H. Berger et al., Phys. Lett. B 35, 87 (1971); W. Bartolet al., Phys. Lett. B 33, 245 (1970); T. Jansens et al., Phys. Rev. 142, 922 (1965); G. Hohler et al., Nucl. Phys. B 114, 505 (1976); F. Borkowski et al., Nucl. Phys. B 93, 461 (1975); R. A. Mold et al., Phys. Rev. Lett. 57, 174 (1986); R. C. Walker et al., Phys. Lett. B 234, 353 (1989).
 - [7] T. A. Armstrong et al., Phys. Rev. Lett. 70, 1212 (1993).
 - [8] A. Antonelli et al., Nucl. Phys. B 517, 3 (1998).
 - [9] M. Ambrogiani et al. [E835 Collaboration], Phys. Rev. D 60, 032002 (1999).
 - [10] M. Castellano et al., Nuovo Cim. A 14, 1 (1973). G. Bassompierre et al., Phys. Lett. B 68, 477 (1977), Nuovo Cim. A 73, 347 (1983); B. Delcourt et al., Phys. Lett. B 86, 395 (1979); D. Bissell et al., Nucl. Phys. B 224, 379

- (1983); Z.Phys.C 48, 23 (1990); G.Bardin et al, Phys. Lett. B 255, 149 (1991); B 257, 514 (1991); Nucl.Phys. B 411, 3 (1994); (1993); A.Antonelli et al, Phys. Lett. B 334, 431 (1994); B 313, 283 (1993).
- [1] J.D.Bjorken, Nucl.Phys.Proc. Suppl. 11, 325 (1989).
- [2] A.Ali, G.Kramer and C.D.Lu, Phys.Rev.D 58, 094009 (1998) [hep-ph/9804363].
- [3] M.Wirbel, B.Stech and M.Bauer, Z.Phys.C 29, 637 (1985).
- [4] M.Bauer, B.Stech and M.Wirbel, Z.Phys.C 34, 103 (1987).
- [5] H.Y.Cheng, C.Y.Cheung and C.W.Hwang, Phys. Rev.D 55, 1559 (1997) [hep-ph/9607332].
- [6] T.E.Browder, K.Honscheid and D.Pedrini, Ann.Rev. Nucl.Part. Sci. 46, 395 (1996) [hep-ph/9606354].
- [7] M.Neubert and B.Stech, hep-ph/9705292.
- [8] H.Y.Cheng and K.C.Yang, Phys.Rev.D 59, 092004 (1999) [hep-ph/9811249].
- [9] R.Machleidt, Adv.Nucl.Phys. 19, 189 (1989).
- [20] J.Speth and R.Tegen, Nucl.Phys.A 511, 716 (1990).
- [21] S.J.Brodsky and G.R.Farrar, Phys.Rev.D 11, 1309 (1975).
- [22] A.A.Logunov, N.Van Hieu and I.T.Todorov, Ann. Phys. 31, 203 (1965).
- [23] V.A.Matveev, R.M.Muradyan and A.N.Tavkhelidze, Lett.Nuovo Cimento 7, 719 (1973).
- [24] V.L.Chernyak and I.R.Zhitnitsky, Nucl.Phys.B 246, 52 (1984).
- [25] R.Baldini, S.Dubnicka, P.Gauzzi, S.Pacetti, E.Pasqualucci and Y.Srivastava, Eur.Phys.J.C 11, 709 (1999).
- [26] H.W.Hammer, U.-G.Meissner and D.Drechsel, Phys. Lett.B 385, 343 (1996) [hep-ph/9604294].
- [27] A.Liesenfeld et al. [ALC Collaboration], Phys.Lett.B 468, 19 (1999) [nucl-ex/9911003].
- [28] P.Mergell, U.-G.Meissner and D.Drechsel, Nucl.Phys. A 596, 367 (1996) [hep-ph/9506375].
- [29] U.-G.Meissner, Nucl.Phys. A 666, 51 (2000) [hep-ph/9907323].
- [30] U.-G.Meissner, Nucl.Phys. A 623, 340C (1997) [hep-ph/9611424].
- [31] V.G.Stoks and T.A.Rijken, Nucl.Phys. A 613, 311 (1997) [nucl-th/9611002].
- [32] W.S.Hou and K.C.Yang, Phys.Rev.D 61, 073014 (2000) [hep-ph/9908202].